RESEARCH ARTICLE

Moist convection and radiative cooling: Dynamical response and scaling

Lokahith Agasthya^{1,2} | Caroline Muller¹

¹Institute of Science and Technology Austria, Klosterneuburg, Austria

²Department of Meteorology and Geophysics, University of Vienna, Vienna, Austria

Correspondence

Lokahith Agasthya, Department of Meteorology and Geophysics, University of Vienna, Vienna, Austria.
Email: lnagasthya@gmail.com

Funding information

European Union Horizon 2020 research and innovation programme MarieSklodowska-Curie, Grant/Award Number: 101034413; European Research Council, Grant/Award Number: ProjectCLUSTER, 805041

ABSTRACT

Moist convection is a fundamental process occurring in the Earth's atmosphere. It plays a central role in the weather and climate of the Tropics, where, to first order, the heating of the atmosphere by convection is in balance with the cooling of the atmosphere by the emission of radiation to outer space. In this study, we use a cloud-resolving model in radiative-convective equilibrium with an imposed constant rate of radiative cooling and study the response of moist convection to varying this rate of radiative cooling. In particular, we study two types of simulation: varying air temperature (VAT) simulations, where the air temperature is allowed to adjust to the imposed radiative cooling, and constant air temperature (CAT) simulations, where the surface temperature is tuned to ensure that the atmospheric temperature profile in the domain is constant. We recover the previously known result that, in response to increasing radiative cooling, the area of convection expands rapidly, while the intensity of convection does not change. We find that this response is explained by the increased boundary-layer variability in simulations with greater radiative cooling, which compensates for the decreasing temperature by adding a larger initial velocity close to the cloud base. We also propose a fundamental scaling of the non-dimensional cumulus mass flux in moist convection, which is robust across models of different complexity. We aim to bridge the gap between highly idealised prototypes of moist convection, such as the "Rainy-Bénard convection" introduced by Vallis et al., and comprehensive cloud-resolving models.

KEYWORDS

moist convection, radiative cooling, fluid dynamics

1 | INTRODUCTION

Convection is an overturning circulation of a fluid (Rayleigh, 1916) driven by vertical differences in density, where denser fluid falls vertically downward while

lighter fluid is lifted vertically upward. In the atmosphere (Emanuel, 1994), convective circulations are usually driven by local heating from the Earth's surface, which leads the layer of air in contact with the surface to be lighter than the air above it, thus rising and bringing

This is an open access article under the terms of the Creative Commons Attribution License, which permits use, distribution and reproduction in any medium, provided the original work is properly cited.

© 2025 The Author(s). Quarterly Journal of the Royal Meteorological Society published by John Wiley & Sons Ltd on behalf of Royal Meteorological Society.

colder air from aloft to the surface through a compensating subsidence. Convection is a leading driver of heat and moisture transport in the Earth system and is particularly important in the Tropics, where deep, moist convection plays a dominant role in determining tropical weather and climate. Convection occurs either in isolated thunderstorms, as part of broader systems (mesoscale convection systems, monsoons), or in conjunction with other synoptic and planetary-scale phenomena, such as equatorial waves, the Madden–Julian oscillation, or the Hadley cell (Houze Jr., 2004; Kiladis *et al.*, 2009; Stevens, 2005; Zhang, 2005).

The Earth's atmosphere loses heat to outer space by (chiefly longwave) radiation (Jeevanjee & Fueglistaler, 2020; Manabe & Strickler, 1964). In the Tropics, the leading-order energy balance is between radiative cooling and the warming of the troposphere by convection, or radiative-convective equilibrium (RCE: Tompkins & Craig, 1998). RCE holds over large enough length- and time-scales in the Tropics (Jakob et al., 2019; Muller & O'Gorman, 2011) and is a key lens used to understand tropical dynamics. Studies of RCE use limited-domain cloud-resolving models (CRMs), where, without large-scale forcing in the steady state, radiation and convection are in equilibrium. CRMs have proved a valuable tool in understanding and gaining insight into several aspects of moist convection and tropical dynamics (Stauffer & Wing, 2022; Wing & Emanuel, 2014), especially the changes in tropical climate in a global warming scenario characterised by higher surface temperatures (Muller et al., 2011; Singh & O'Gorman, 2015). Behaviour observed in CRMs has instigated studies into realistic models and observations (Holloway et al., 2017; Wing et al., 2017). The utility of CRMs, however, goes well beyond mean-state tropical dynamics. CRMs can be used in non-RCE configurations, with the boundary conditions and energetic and mass balances configured to mimic real-world conditions and the influence from large scales on limited-area models (Singh & Neogi, 2022).

Convection warms the atmosphere by transporting heat upwards, mainly by the transport of water vapour (or latent heat), which condenses (and freezes) aloft in the atmosphere. The convective transport of latent heat occurs via rising cloud plumes, in which the air is saturated with moisture. The dynamics of these plumes is set by complex, nonlinear mutually interacting cloud processes involving both the large-scale conditions and the microphysics of water condensates (Arakawa & Schubert, 1974; Arakawa & Wu, 2013). A commonly used measure for the strength of convection is the rate of upward transport of air within cloud plumes, or the cloudy mass flux (known henceforth simply as the mass flux). Under RCE, the greater the radiative cooling, the greater the mass flux. The mass flux $M_{\rm c}$ at a given height can be written as

$$M_{\rm c} = \rho \sigma w_{\rm c},\tag{1}$$

where ρ is the density of dry air, σ_c is the area fraction of the horizontal cross-section that is occupied by clouds, and w_c is the typical vertical velocity within these clouds.

The scaling of the mass flux with changes in radiative cooling has been studied previously in CRMs (Robe & Emanuel, 1996; see also similar simulations by Cohen & Craig, 2006), where it was found that, while M_c increased strongly with the imposed rate of radiative cooling R, this increase occurred by an increase in the area of clouds (i.e., increase in σ), while the intensity of updraughts in the clouds (i.e., w_c) remained nearly constant. This scaling has also been observed in other numerical simulations, for example, in Shutts and Gray (1999; see their figures 7, 8, and table 1) and Parodi and Emanuel (2009; see their fig. 8 showing updraught velocity for large changes in the radiative cooling). Further, the dynamic consequences of the expanding area of convection and constant vertical velocity in clouds in response to increased radiative cooling are reviewed in Yano and Plant (2012). More recently, the response of dry and moist convection to varying rates of bulk cooling was studied in idealised two-dimensional (2D) direct numerical simulations (Agasthya et al., 2025; Agasthya & Muller, 2024). In Agasthya et al. (2025; henceforth AMC25), using the Rainy-Bénard model of moist convection (Vallis et al., 2019) the study found that the same scaling in response to radiative cooling holds even in highly idealised 2D settings, establishing that this scaling is a fundamental feature of moist convection and not the consequence of parametrised subgrid-scale processes or set by the microphysics of liquid water and ice.

In this study, we revisit the simulations of Robe and Emanuel (1996; henceforth RE96) and study the scaling of moist convection in the light of several new findings around moist convection in the intervening time of three decades. In addition to changing the mass flux, increased radiative cooling affects domain-mean temperatures, with more cooling leading to a colder domain. Here, we decouple the changes in the dynamics due to the changing temperature of the domain from the changes due to the altered circulation caused by varying radiative cooling. Further, we use the fundamental insights gained from idealised models to understand changes in cloudy area, arguing that fundamental constraints from convective dynamics and the changes in the boundary layer lie at the heart of the widespread convection seen in simulations with large radiative cooling. Finally, we identify that the average velocity in clouds is a fundamental velocity scale. Using this velocity scale, we show that, in idealised moist convection, a simple power-law scaling exists between the non-dimensionalised mass flux

onditions) on Wiley Online Library for rules of use; OA articles are governed by the applicable Creative Commons License

and the non-dimenionsalised ratio of radiative cooling to condensation heating.

The rest of the article is organised as follows. Section 2 details the cloud-resolving model used for our RCE studies and the numerical experiments performed. Section 3 outlines the main results and scientific insights gained from these simulations. In Section 4, we summarise our work and point to potential future avenues of research.

2 | METHODOLOGY

We perform RCE simulations using the System for Atmospheric Modeling (SAM: Khairoutdinov & Randall, 2003) version 6.10.8. SAM uses anelastic momentum and scalar advection-diffusion equations with prognostic thermodynamic equations for liquid water/ice static energy, total precipitating water, and total non-precipitating water. Microphysical processes are parametrised using one-moment microphysics, while subgrid-scale turbulence closure is parametrised using a Smagorinsky-type parametrisation (as in Bretherton et al., 2005; Muller & Held, 2012). Surface fluxes are parametrised using bulk formulas based on Monin-Obukhov similarity. The equations are solved on a 128 km × 128 km horizontally periodic square domain with horizontal grid spacing of 1 km. The domain is 27 km high, with a sponge layer with Newtonian damping on all prognostic variables to absorb gravity waves in the top 9 km. There are a total of 64 vertical levels, with 53 in the first 18 km including nine levels in the lowest km. The lowest atmospheric model level is at 37.5 m and the vertical resolution decreases with height to 400 m in the mid and upper troposphere. A constant radiative cooling rate -R K · d⁻¹ is imposed up to a height of 10 km, above which it is gradually relaxed to zero at a height of 14 km. We set the stratosphere to be at a constant temperature of 200 K. Where the temperature is lower than this value, the temperature is nudged to 200 K with a time-scale of two days. This leads to a uniform cooling in most of the troposphere, while maintaining stratospheric temperatures close to 200 K (similar to Pauluis & Garner, 2006).

The first set of five simulations is performed with a sea-surface temperature (SST) of 300 K and the magnitude of the imposed radiative cooling R varying from 0.75–7.2 K·d⁻¹. In line with expectations and RE96, we find that the average air temperature in the domain decreases in response to a stronger cooling. Thus, any changes observed in the flow when R is increased could be due to changes in the circulation due to the direct effect of R or an indirect effect of the change in air temperature. To isolate the former dynamic response from the latter thermodynamic response, we perform an additional set of

simulations where the SST is tuned by having a larger SST for simulations with larger R. This SST tuning ensures that the temperature of the lowest atmospheric level in the model T_a is within less than 1 K of that in the simulation with SST of 300 K and $R = 1.5 \text{ K} \cdot \text{d}^{-1}$. This tuning leads the average air temperature profile to be nearly identical across simulations with different R. Henceforth, the first set of simulations with SST of 300 K and varying R will be known as the varying air temperature (VAT) simulations. The second set of simulations with SST tuned such that the air temperatures are identical will be known as the constant air temperature (CAT) simulations. The reader must note that the simulation with SST = 300 Kand $R = 1.5 \text{ K} \cdot \text{d}^{-1}$ is common to VAT and CAT and is henceforth referred to as the control simulation (CTRL). All simulations are run until they reach a steady state and all analysis is performed after that transient period using 50 days of steady-state dynamics.

3 | RESULTS

3.1 | Response of temperature, moisture, and mass flux

The imposed SST and various important simulation quantities are summarized in Table 1, while Figure 1 shows the relative changes in sensible heat flux (SHF), latent heat flux (LHF), and their sum plotted against the relative change in R. In our simulations, R ranges from $0.75-7.2 \text{ K} \cdot \text{d}^{-1}$ —this corresponds to a 9.6-fold increase, or a relative change of 8.6. For the VAT simulations, T_a shows a sharp decrease with increasing R and the domain gets colder. The surface heat fluxes increase rapidly to balance the cooling in the domain. The sensible heat flux increases faster than R, while the latent heat flux increases slower than *R* (below the y = x line). This can be attributed to the fact that sensible heat becomes more important as the domain becomes colder and drier. It is also important to note that the net flux (SHF + LHF) for the VAT simulations increases slightly more slowly than the increase in R. This is because, when the domain becomes colder, the convection becomes shallower and the stratospheric temperature of 200 K is reached at a lower height in the atmosphere. This leads to a slower increase in the column integrated radiative cooling compared with R, and the fluxes respond accordingly.

As noted in Section 2, the CAT simulations have different SSTs but the resulting T_a are nearly the same, within < 1 K of each other. For larger R, the CAT simulation domains have nearly identical temperature and moisture to CTRL. Here (see light green curves), the increase in LHF scales exactly with the increase in R, while the SHF

The imposed value of $R(K \cdot d^{-1})$ and SST (K) for the VAT and CAT simulations. The various averaged quantities shown are the lowest atmospheric level temperature T_a (K), surface sensible heat flux SHF, and surface latent heat flux LHF (both in W m⁻²), respectively.

	Varying	Varying air temperature (VAT)				Constant air temperature (CAT)			
R	SST	T_{a}	SHF	LHF	SST	T_{a}	SHF	LHF	
0.75	300	297.98	6.41	66.62	296.8	294.35	7.66	61.03	
1.5	300	294.56	20.82	118.73	300	294.56	20.82	118.73	
2.0	300	292.28	31.89	149.11	302	294.88	29.75	160.85	
3.6	300	286.71	72.97	240.29	305.8	294.16	53.91	285.40	
7.2	300	279.91	165.06	401.20	312.5	293.90	109.82	579.46	

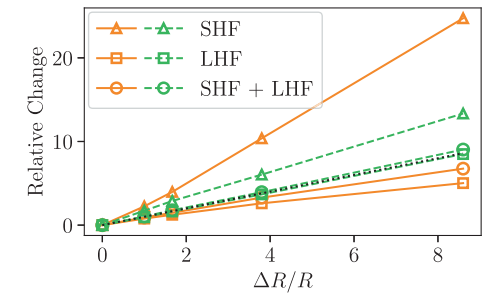


FIGURE 1 The figure shows the relative change of surface sensible heat flux (SHF, triangles), latent heat flux (LHF, squares), and their sum (SHF + LHF, circles), plotted against the relative change in radiative cooling. The orange solid curves and light green dashed curves show the scaling for VAT and CAT simulations, respectively. The black dotted line shows the y = x line for reference. [Colour figure can be viewed at wileyonlinelibrary.com]

shows a superlinear increase. The total surface flux thus increases marginally faster than R. The larger relative increase in SHF is due to the domain becoming slightly drier (smaller relative humidity) and the convection in the domain reaches slightly higher altitudes due to small changes in the temperature profile.

The time-averaged vertical profiles of temperature T, water-vapour mixing ratio q_v , and relative humidity are shown in Figure 2. In the VAT simulations (top panels of Figure 2), for increasing R (darker shades of blue) the temperature in the domain decreases significantly, also leading to a decrease in q_v as well as large variations in the relative humidity profiles. We note in passing that the profiles shrink vertically with cooling, consistent with previous work (Singh & O'Gorman, 2012). The profiles show consistency when plotted using temperature as a vertical coordinate (Jeevanjee, 2022, also see Appendix A), a theme that we will return to later.

For CAT simulations, we see that not only the lowest model level temperature but also the temperature profiles of all the simulation domains are very close to each other and are nearly indistinguishable from each other in the plotted figure. Though temperature differences of

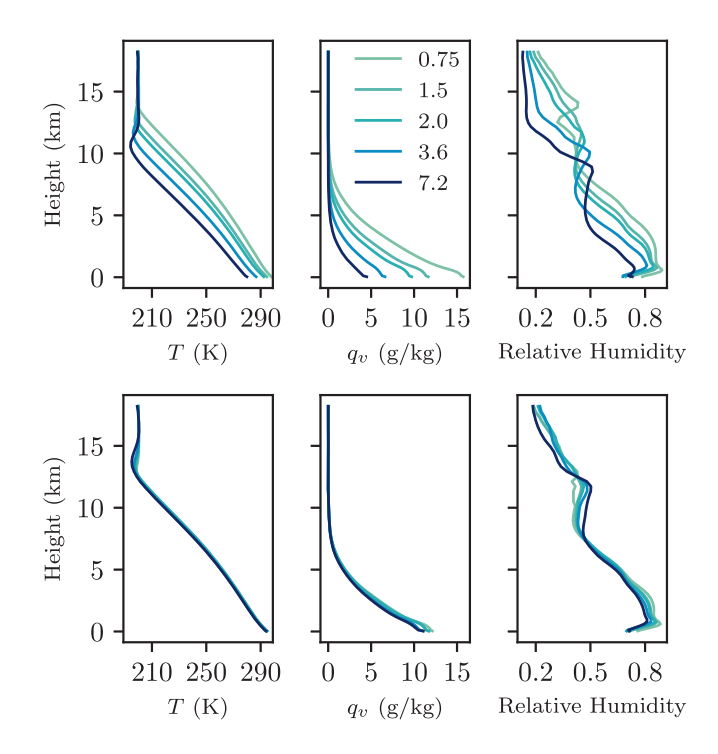


FIGURE 2 From left to right: horizontal and time-average profiles of temperature, water-vapour mixing ratio, and relative humidity for the five values of R (values shown in legend with units $(K \cdot d^{-1})$ with VAT (top panels) and CAT (bottom panels). [Colour figure can be viewed at wileyonlinelibrary.com]

the order of 2 K are present, this is a first indication that the temperature profile, which is in turn set by convection, is a function of surface temperature and moisture, independent of the radiative cooling.

As discussed in RE96 and AMC25, greater radiative cooling leads to an increase in the magnitude of the average subsiding vertical velocity w_{sub} outside clouds. This subsidence is radiatively driven and the subsidence adiabatic warming plays an important role in balancing the imposed cooling. From the conservation of mass, w_{sub} is related to the cloud mass flux at a given height as

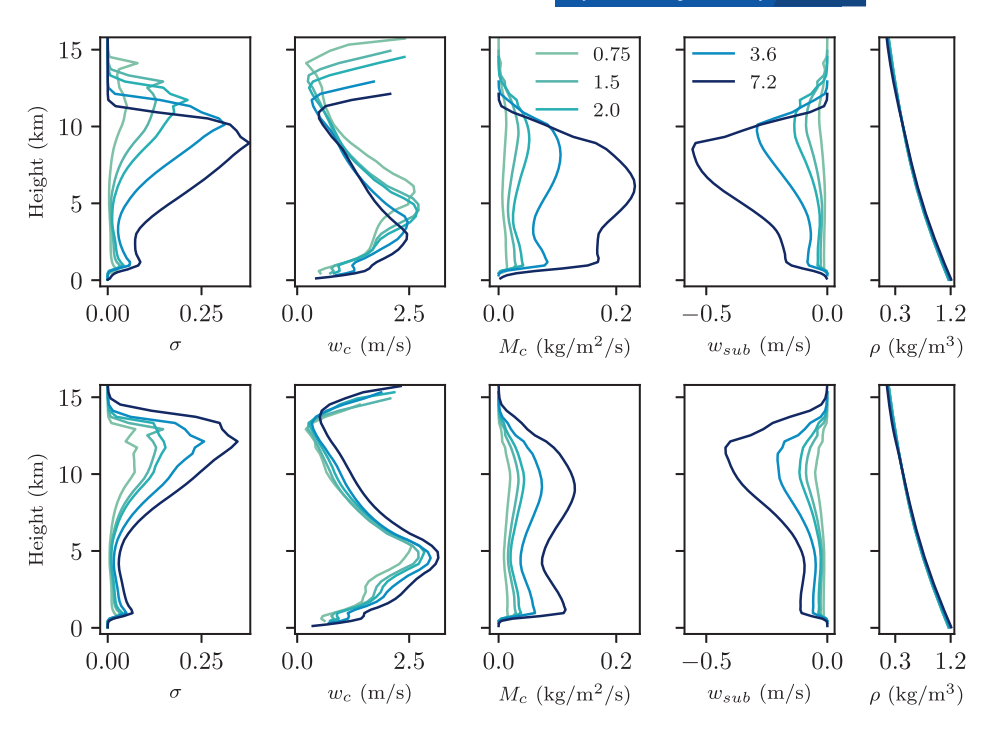
$$M_{\rm c} = \overline{\rho} \sigma w_{\rm c} = \overline{\rho} (1 - \sigma) |w_{\rm sub}|, \tag{2}$$

1477870x, 0, Downloaded from https://rme

nlinelibrary.wiley.com/doi/10.1002/qj.70044 by Institute Of Science And Technology Austria, Wiley Online Library on [20/10/2025]. See the Terms and Conditions (https://doi.org/10.1002/qj.70044 by Institute Of Science And Technology Austria, Wiley Online Library on [20/10/2025]. See the Terms and Conditions (https://doi.org/10.1002/qj.70044 by Institute Of Science And Technology Austria, Wiley Online Library on [20/10/2025]. See the Terms and Conditions (https://doi.org/10.1002/qj.70044 by Institute Of Science And Technology Austria, Wiley Online Library on [20/10/2025]. See the Terms and Conditions (https://doi.org/10.1002/qj.70044 by Institute Of Science And Technology Austria, Wiley Online Library on [20/10/2025]. See the Terms and Conditions (https://doi.org/10.1002/qj.70044 by Institute Of Science And Technology Austria, Wiley Online Library on [20/10/2025]. See the Terms and Conditions (https://doi.org/10.1002/qj.70044 by Institute Of Science And Technology Austria, Wiley Online Library on [20/10/2025]. See the Terms and Conditions (https://doi.org/10.1002/qj.70044 by Institute Of Science And Technology Austria, Wiley Online Library on [20/10/2025].

ditions) on Wiley Online Library for rules of use; OA articles are governed by the applicable Creative Commons License

FIGURE 3 From left to right: time and horizontally averaged profiles of cloudy area fraction, average vertical velocity in clouds, cloudy mass flux, average vertical velocity outside clouds, and dry air density, for (top panels) varying air temperature and (bottom panels) tuned air temperature simulations. A grid point is considered to be cloudy if the mixing ratio of non-precipitating water (cloud water + cloud ice) $q_n > 10^{-5} \text{ g} \cdot \text{kg}^{-1}$ and w > 0. [Colour figure can be viewed at wileyonlinelibrary.com



where the line over ρ indicates that it is the anelastic density profile, which is a function of height alone. Here $w_{\rm sub}$ is the vertical velocity averaged only over regions that are not clouds, while $w_{\rm c}$ and σ are the vertical velocity averaged within clouds and the area fraction of clouds, respectively. Away from clouds, assuming a balance between radiative cooling and subsidence warming yields (e.g., Robe & Emanuel, 1996)

$$w_{\rm sub} = \frac{-R}{(T/\theta)\partial_z \theta} \equiv \frac{-R}{S},$$
 (3)

where θ is the potential temperature and S is known as the dry stability of the column, which is proportional to the difference between the dry and moist adiabatic lapse rates (Bony *et al.*, 2016; Jeevanjee, 2022). This suggests that, up to changes in stability (which can be significant), the subsidence velocity must scale proportionally with the radiative cooling.

Henceforth in our analysis, we define a grid point to be "cloud" if it is rising (w > 0) and has a non-precipitating condensate mixing ratio q_n greater than 10^{-5} kg · kg⁻¹, a fairly standard definition of a cloud in the literature. Figure 3 shows the time- and horizontally averaged profiles of σ , w_c , M_c , $w_{\rm sub}$, and ρ . In the top panels showing the averages of the VAT simulations, we recover the result that, while the mass flux increases rapidly with stronger radiative cooling, w_c remains fairly constant, showing a mid-tropospheric maximum that is insensitive to R. The profiles of ρ also remain nearly constant across the simulations. The increase in mass flux is then driven by the large increase of σ —the mass flux increases by having more

clouds with the same intensity of convection. On the flip side, $w_{\rm sub}$ also shows a large increase with increasing R, closely mirroring the increase in mass flux, as expected from Equation (3). Here, S decreases for simulations with larger R, as the domain becomes drier and the dynamics approach dry convection. It is important to note here that the convection becomes shallower for increasing R in the VAT simulations. This can be gauged either by observing the peaks of $w_{\rm c}$ and $w_{\rm sub}$ or by noticing that σ goes to 0 in the upper troposphere closer to z=14 km for R=0.75 K·d⁻¹, while this happens closer to z=11 km for z=1.75 K·d⁻¹. This becomes important when comparing convective quantities at a given height, something we will come back to later.

The same profiles from the CAT simulations are shown in the lower panels of Figure 3. Here too, the increase in mass flux with increasing R is pronounced and this increase is driven mainly by the increase in σ , an increase that is also seen in the magnitude of $w_{\rm sub}$. However, $w_{\rm c}$ shows a small, monotonic increase at every height up to ~ 12 km, the highest value occurring at nearly the same height across the simulations. The maximum $w_{\rm c}$ shows a monotonic increase; however, the fractional increase in this peak is still small compared with the increase in R or σ —merely a $\sim 25\%$ increase for a 9.6 times larger forcing (or 860% increase) and a 12.5 K warmer SST.

This is accompanied rather puzzlingly by a decrease of convective available potential energy (CAPE) by 80% (or five times smaller) for the VAT simulations and an 18% decrease in CAPE for CAT simulations. CAPE is a measure of the potential energy for convection in a given column of the atmosphere. CAPE is defined as the positive part of the

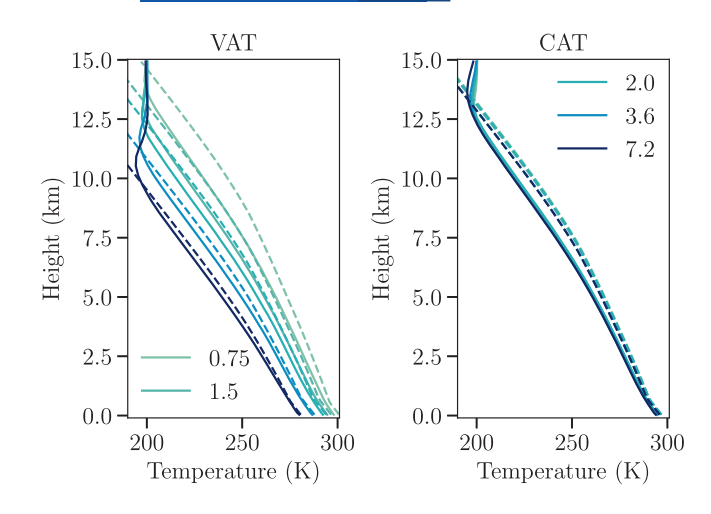


FIGURE 4 Domain-average temperature profiles (solid lines) and the virtual temperature of the idealised, moist adiabatic (dashed lines) for VAT and CAT simulations. [Colour figure can be viewed at wileyonlinelibrary.com]

buoyancy of a moist-adiabatic parcel lifted from the surface and is known to be strongly associated with intense convective activity and thunderstorms (Johns & Doswell III, 1992). The temperature profiles of the moist adiabats and the corresponding domain-average temperature profiles are shown in Figure 4. CAPE decreases in the VAT simulations because of a significant decrease in temperature and moisture available for convection. This leads to a decrease in both the saturation deficit (or the distance between the average temperature profile and the moist adiabat) and the height of the level of neutral buoyancy (the height in the upper troposphere at which the moist adiabat intersects with the average temperature profile). In the CAT simulations, the decrease is due to small changes in relative humidity and q_v in the domain (see lower middle and right panels of Figure 2), leading to a slight leftward shift in the moist-adiabatic profile (dashed curves of the right panel) with increasing R. Thus, we see a decrease in CAPE but an overall increase in the average vertical velocity in clouds.

Given that CAPE is usually associated with extreme events rather than average clouds, we also assess the extreme vertical velocity. We consider the 99.99th percentile of w at each height and then choose the maximum such 99.99th percentile w. This peak value typically occurs higher up in the troposphere (8–13 km) compared with the peak in w_c . This value also shows a monotonic increase of 68% in CAT (profile not shown). For VAT, the increase from the simulation with the smallest R to that with the largest R is \sim 32%, though this increase is not monotonic. Instead, the peak lies between 19 and 21.5 m \cdot s⁻¹ in all the simulations except that with the smallest R. Other extreme values of w also show similar variations with R. It remains

to be seen why, despite a large increase in surface forcing and a strengthening of the circulation with a strong subsidence flow, w_c increases by only a small amount, a change opposite in sign to the change in the moist instability as traditionally measured by CAPE.

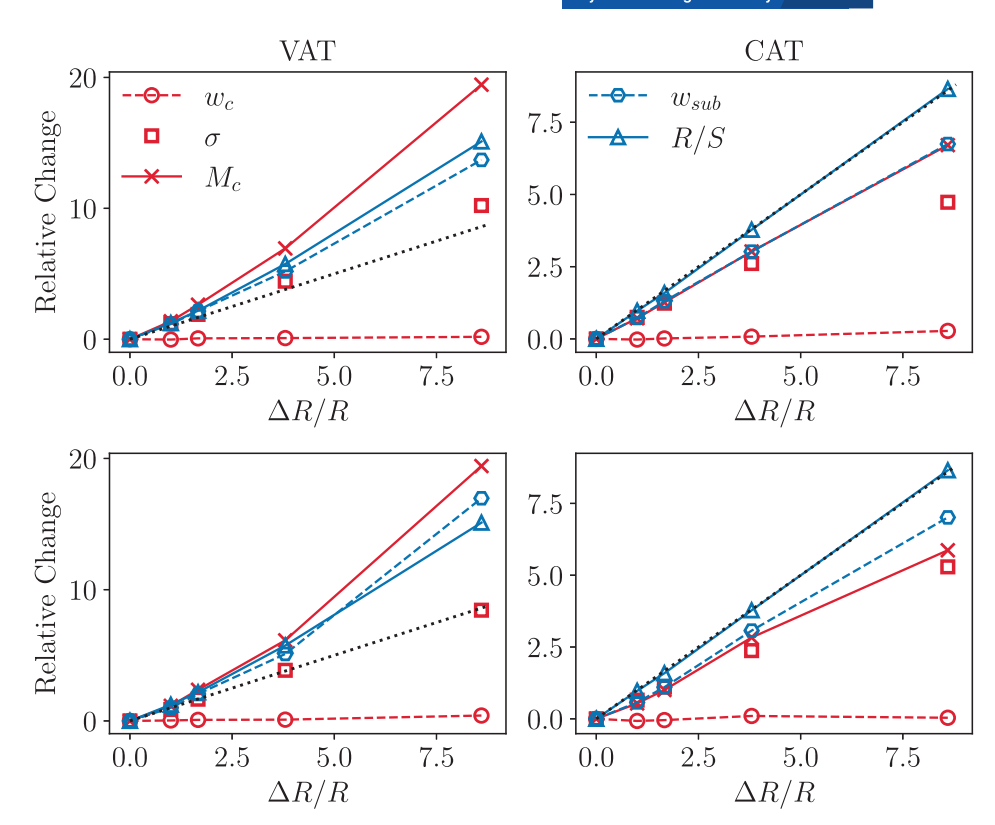
3.2 | Relative changes in convective quantities

To understand the precise scaling of these quantities with the changes in radiative cooling, in the top panels of Figure 5 we plot their relative (or fractional) changes against the relative change in R for VAT (left) and CAT (right) simulations. The plots also have the black, dotted y = x straight line for reference, as a linear relationship would lie on this curve. The relative changes of the quantities w_c , σ , M_c , w_{sub} , and R/S are plotted at a given temperature level rather than a chosen vertical height. While these quantities have previously been compared at a fixed height (for example a height of 6.7 km in RE96), we argue that the temperature level is a better way to ensure like-for-like comparisons (Jeevanjee, 2022). This is discussed further in Appendix A. We choose the 250-K temperature level for our analysis. This temperature level corresponds to a regime well above the boundary layer and lifting condensation level (LCL) in all simulations, while also being well below the cloud anvil across the simulations. The 250-K level in CTRL corresponds to a height ~ 6.5 km, which is comparable with the height chosen by RE96 for their analysis. We note that the results are qualitatively similar for temperature levels between 265 and 235 K.

The scaling for the VAT case is nearly identical to the scaling seen in fig. 3a of AMC25, with the mass flux (solid curve, crosses) increasing faster than R (a superlinear increase), the area of convection (square markers) increasing linearly with R, and the velocity within clouds showing very little change (dashed curve, circular markers). Outside clouds, the subsidence velocity (solid curve, triangles) scales similarly to the predicted R/S scaling where S is calculated from the mean vertical temperature profile. In colder domains, S is smaller, leading to a superlinear increase of R/S with R. Given that the changes are measured at the same temperature level, a small part of the increase in M_c can also be attributed to the change in density, where, for the simulations with larger R, the 250-K level is lower down in the domain and thus the density of air is also larger.

In the CAT simulations, all the domains have the 250-K level at the same height and thus the changes are purely due to the changes in the circulation and convection, which are the result of the changing *R*. Here the mass flux increases slightly more slowly than linearly, exactly with

FIGURE 5 Relative change of various quantities in (left) VAT and (right) CAT simulations plotted against relative change in R linearly interpolated to the temperature level T = 250 K within each simulation (note the change in y-axis range across panels). This corresponds to ~ 6.5 km in CTRL and all CAT simulations, while it varies from 7.6-3.8 km in VAT simulations. The relative changes plotted in the upper panels are average vertical velocity in clouds w_c , cloud area fraction σ , cloud mass flux M_c , average vertical velocity outside clouds w_{sub} , and radiative cooling R divided by stability S. The lower panels show the same, but for convective regions (see main text for definition). All panels have the y = x black, dotted curve for reference. [Colour figure can be viewed at wileyonlinelibrary.com]



 $w_{\rm sub}$. Here too, as in the VAT simulations, the changes in mass flux are closely tied to changes in σ , with changes in $w_{\rm c}$ contributing little to the change in $M_{\rm c}$. R/S scales linearly with R, as the temperature profiles of the simulations are nearly identical, thus the stability (proportional to the gradient of the temperature profile) also does not change significantly across different simulations.

While w_{sub} broadly scales with R/S, we must note here that the magnitudes of the two quantities do not show a very good match. Figure 6 shows the average subsidence velocity w_{sub} outside clouds (solid, blue curves). It is seen here that there is a large mismatch between this value (blue) and the prediction from a pure radiative balance (green, dashed curve). This match does not improve greatly when the cooling due to the re-evaporation of falling rain is also included (dotted, brown curve) in the prediction, as suggested by Jeevanjee (2022). The mismatch is especially large near the cloud anvil—here, convergence outside clouds is known to play a stronger role in producing subsidence velocities (Bony et al., 2016). However, we found that including the horizontal convergence term still does not improve the prediction (not shown). Previous work (Jeevanjee & Zhou, 2022) has shown that cooling due to evaporation of cloud condensates near the cloud anvil (see their appendix C), often neglected, contributes significantly to the acceleration of downdraughts. We do not verify whether this holds in our simulations.

The fact that even the mid-tropospheric values do not match well with radiative equilibrium indicates that looking at vertical velocities purely outside clouds is not a good measure for purely radiation driven subsidence. A cloud here is a pointwise metric requiring a threshold value of non-precipitating condensate mixing ratio and rising motion (w > 0). In the mid-troposphere, the mismatch is likely due to the large degree of turbulent vertical velocity fluctuations and strong return flows near the clouds, which are related to the cloudy dynamics rather than subsidence in clear-sky regions far away from clouds.

Thus, we instead turn our attention to "convecting regions". A vertical column is defined to be part of the convecting region if the column-integrated cloud water (CICW) is above a threshold of $0.5 \text{ kg} \cdot \text{m}^{-2}$ (the results remain unchanged for a broad range of thresholds from 0.1-1 kg \cdot m⁻²). The regions of high CICW are co-located with regions of high column-integrated precipitable water, high surface precipitation, and high mid-tropospheric vertical velocity, indicating that these are regions of intense convective activity, even if momentarily they lack condensates at some height. Figure 6 shows that the average subsidence outside these regions matches closely with pure radiative equilibrium in the mid-troposphere. Thus, pure radiatively driven subsidence can be seen outside convecting regions, rather than outside clouds alone.

0 + -0.05

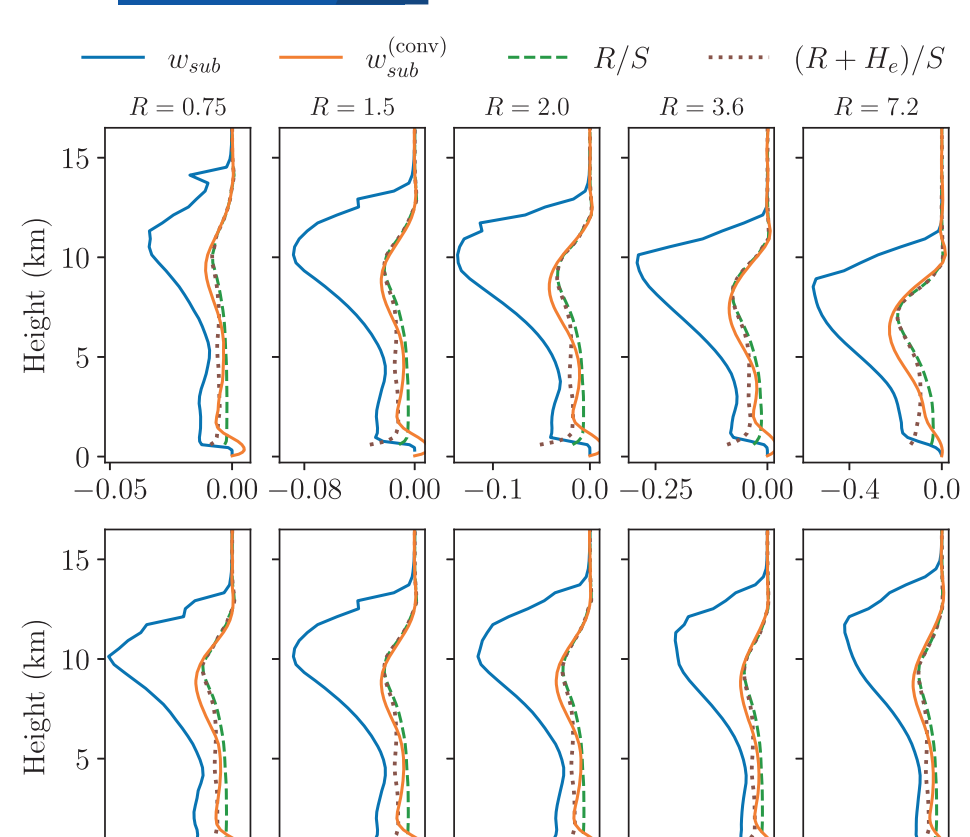


FIGURE 6 Time and horizontally averaged profiles of vertical velocity in m · s⁻¹ outside clouds (solid blue curve) and outside convective regions (solid orange curve) compared with the prediction of pure radiative balance R/S(dashed green curve) and a radiation + reevaporation balance (dotted brown curve) in VAT simulations (top panels) and CAT simulations (bottom panels) for all the studied values of R in $K \cdot d^{-1}$ as indicated by the plot titles. Note that the x-axis ranges vary for different R. [Colour figure can be viewed at wileyonlinelibrary.com

The lower panels of Figure 5 show the scaling of average vertical velocity and the mass flux within convecting regions, as well as the area fraction occupied by these regions at the same temperature level as the upper panels (250 K). In other words, we performed the same analysis as above using the column-integrated threshold to identify convective regions instead of clouds identified by a pointwise metric. All these three quantities (shown in red) scale nearly identically in the upper and lower panels for VAT as well as CAT. This crucial fact indicates that, across simulations, the clouds have very similar structures and, for instance, the ratio between the cloud fraction and the convecting area fraction remains fixed at a given temperature level.

0.00 - 0.08

0.00

-0.1

0.0 - 0.25

0.00

-0.4

0.0

The picture that emerges is that of rising, saturated cloud plumes, with the area occupied by them expanding to increase their mass flux, while the dynamics within them is fairly constant. These cloud plumes carry with them a region of intense activity which is not radiatively driven. These regions are not cloudy—they consist of either unsaturated regions or saturated parcels of downward-moving air (w < 0), hence not satisfying the criteria we have adopted for a cloud. However, they are still strongly influenced by the dynamics of the saturated plumes due to their close proximity to them. We refer to

these regions as "cloud baggage". (See also the discussion on the related concept of "inactive air" introduced by Seeley *et al.*, 2019 to refer to downward-moving or slowly upward-moving saturated parcels of air). This "cloud baggage" also scales linearly with the cloud plumes, so that, when taken together, the cloud plumes and their baggage form the "convecting regions" of the flow, responsible for clouds and precipitation. Outside these convecting regions, the dynamics is simply in balance with radiative cooling and feels the imprint of the varying R directly. The fact that the baggage is "well-behaved" is rather fortuitous, allowing the direct comparison of the vertical derivatives of R/S (or $(R + H_e)/S$) with the vertical derivative of w_{sub} measured outside clouds (Bony *et al.*, 2016; Jeevanjee, 2022).

The invariance of w_c across simulations, taken together with the linear scaling between the properties of the cloud plumes and the cloud baggage, suggests that the properties of the clouds, such as the area occupied by individual clouds, do not change much. Instead their numbers simply increase. Previous studies that varied R in similar CRM setups do find that the increase in cloudy area fraction is due to an increase in the number of clouds, while the distribution of the sizes of cloud cores does not vary (Cohen & Craig, 2006; Craig & Cohen, 2006).

3.3 | Vertical variation in cloud characteristics

To understand the processes that set w in clouds better, we assess the buoyancy within clouds. The lower panels of Figure 7 show the histogram of buoyancy at the 250-K level for the VAT and CAT simulations. We see here that the distribution of buoyancy does not show large differences, with even the tails of the distributions showing little difference in the CAT case. In the VAT case, the cases with larger R actually have smaller positive tails, consistent with the decrease in temperature and hence moisture and CAPE, leading to a smaller ability to create large positive buoyancies. This, however, is contrary to the observed small increase in w_0 as well as extreme values of w with R.

The distribution of buoyancy at $z \sim 600$ m (top panels), on the other hand, shows large differences with varying R. This height corresponds to the first height at which the average cloud fraction is above 0.1% in all simulations, ensuring that the histogram is reasonably smooth. It corresponds to the sixth model level, which is close to the theoretical LCL for all the simulations (between the fifth and sixth levels). It is below the lower-tropospheric peak of cloud fraction in all but one simulation ($R = 0.75 \text{ K} \cdot \text{d}^{-1}$), so it represents a regime at or just below the cloud-base level, where the dynamics is influenced strongly by the boundary layer. At this level, the buoyancy histogram shows sharp differences, with the positive and negative anomalies being much larger for the simulations with large R in both sets of simulations. With increasing R,

the distribution also becomes flatter and the tails are more pronounced. The inset to the top right panel shows the vertical velocity within clouds at the same height, which we denote $w_c^{(b)}$. Here, unlike its mid-tropospheric counterpart, $w_c^{(b)}$ shows a noticeable increase with increasing R, showing an approximately threefold increase in value in both sets of simulations.

The above discussion, while holding many insights into the scaling of moist convection, still does not address the vexing central question: why does the area alone expand rapidly with increasing R? Changing the radiative cooling impacts a host of different flow characteristics, including the surface fluxes, the domain mean temperature, the relative humidity, and the stability. One set of quantities that remains remarkably constant across the simulations is the vertical variations in the various cloud characteristics considered in the preceding paragraphs. In particular, the vertical gradients in σ , w_c , M_c , and w_{sub} plotted using temperature as a vertical coordinate, shown in Figure 8, follow almost exactly the same curves above the boundary layer in the mid- and upper-troposphere, with large differences closer to the boundary. This shows that all these quantities have the same vertical structure and a common vertical form function, independent of the forcing. Any inter-simulation differences, then, must arise from differences that already exist at the top of the boundary layer.

Thus, instead of looking at the scaling of the velocity in clouds alone, in Figure 9 we plot various other quantities related to the vertical velocity along with w_c . The 99.99th

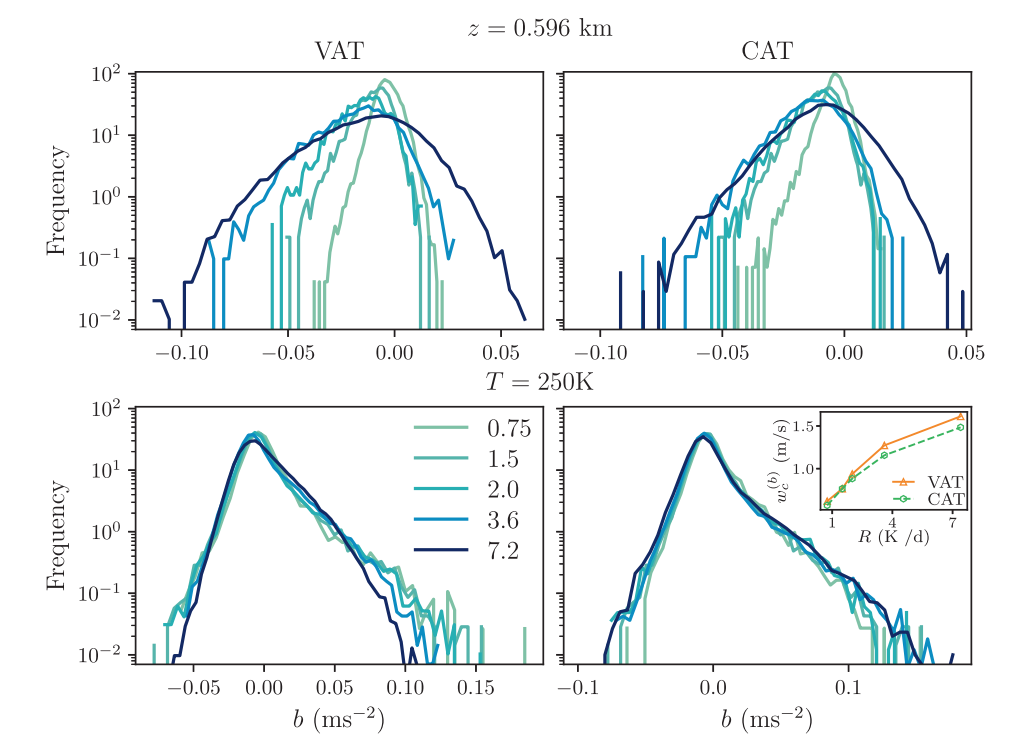


FIGURE 7 Histogram of the buoyancy in clouds in the boundary layer (z = 596 m, top panels) and temperature level closest to T = 250 K (lower panels) for simulations with different R for VAT (left) and CAT (right). The inset in the lower right panel shows the boundary-layer vertical velocity $w_c^{(b)}$ at the same height. [Colour figure can be viewed at wileyonlinelibrary.com]

10 of 16 Quarterly Journal of the RMetS AGASTHYA and MULLER

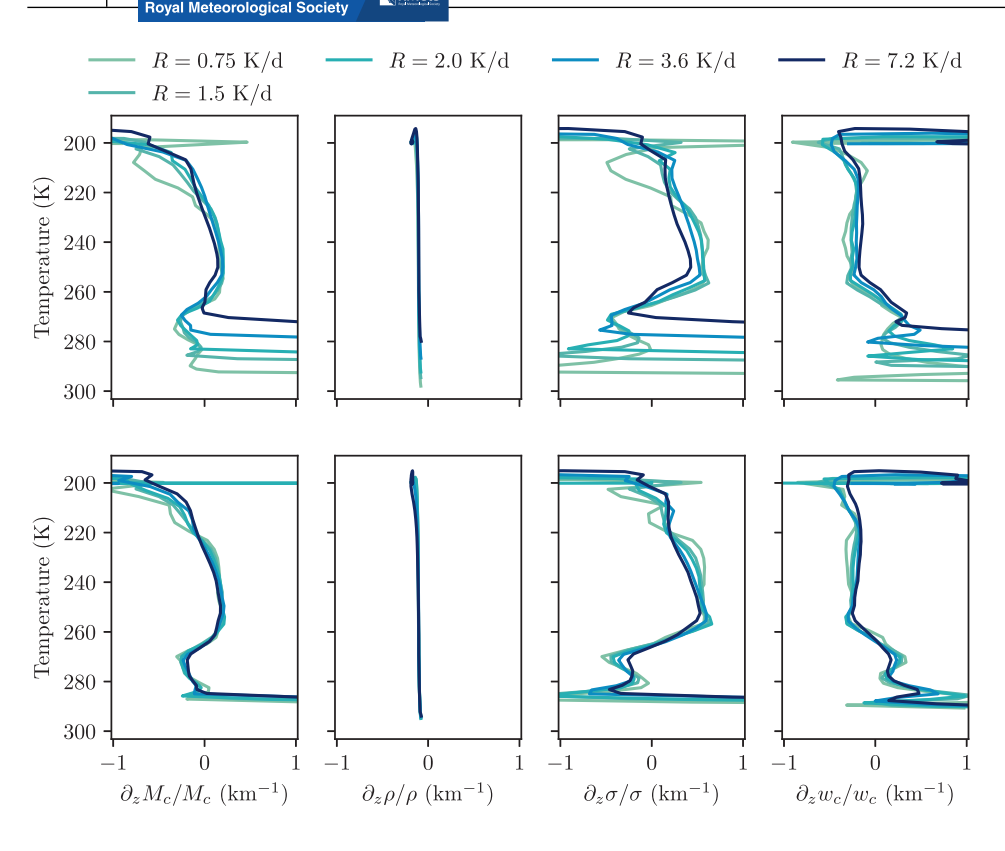


FIGURE 8 Plots showing the fractional rate of vertical change for M_c , ρ , σ , w_c , for VAT (upper panels) and CAT (lower panels), plotted on isothermal coordinates. [Colour figure can be viewed at wileyonlinelibrary.com]

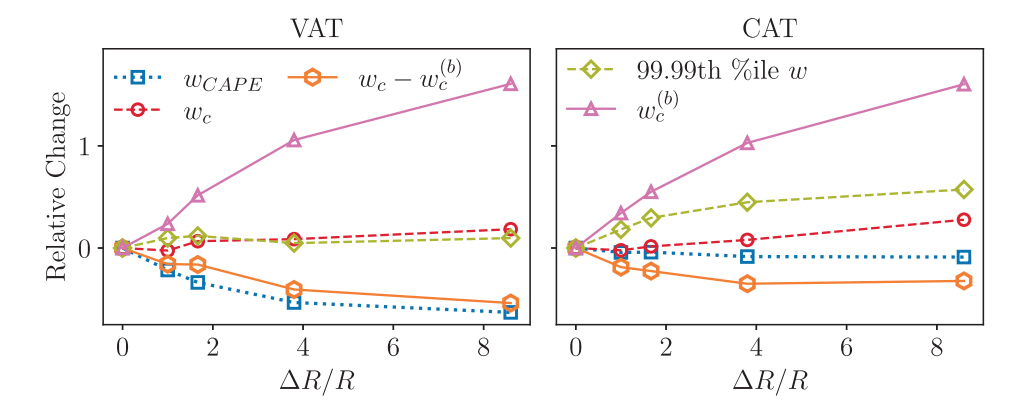


FIGURE 9 The relative change in various quantities plotted as a function of the relative change in R for varying air temperature and tuned air temperature simulations linearly interpolated to the T = 250-K level. See main text for definitions. [Colour figure can be viewed at wileyonlinelibrary.com]

percentile of vertical velocity is shown to scale similarly to w_c . w_{CAPE} is the prediction of w from the CAPE, that is, the vertical integral of the buoyancy of a moist adiabatic parcel lifted from the surface up to the given temperature level. As stated earlier, CAPE decreases with R in both simulations. Finally, we show the scaling of w_c with the contribution of the top of boundary-layer vertical velocity, or $w_c^{(b)}$, removed. $w_c - w_c^{(b)}$ is thus a measure of the acceleration in clouds above the boundary-layer height, here taken to be 596 m. We have already seen in the inset of Figure 7 that this value responds quite strongly to R. Here we see that the scaling of $w_c - w_c^{(b)}$ (green curve) closely follows the scaling of the prediction from CAPE (blue curve) in the VAT and CAT cases. This scaling works similarly well for temperature levels below and close to the peak in the vertical profile of w_c . Above this level, the

value of w_c starts to decrease while the moist adiabat is still positively buoyant and it would be unphysical to continue to compare these curves. We note here that the peak in the extreme cloud velocities occurs far higher up in the domain, closer to the 230-K temperature level and higher.

This shows that the apparent insensitivity of w_c to CAPE is actually a boundary effect. Even as the boundary becomes colder and drier, decreasing the moist instability and CAPE, the increasingly unstable boundary layer, strongly driven by the stronger surface fluxes, leads to large variability in the boundary layer, creating strongly accelerated, upward-moving parcels at the cloud base itself. Above the cloud base, the on-average incremental upward acceleration is related to the more traditional instability measure of CAPE. The increased boundary-layer variability is seen not only in the buoyancy distribution but also

1477870x, 0, Downloaded from https://rmets.onlinelibrary.wiley.com/doi/10.1002/qj.70044 by Institute Of Science And Technology Austria, Wiley Online Library on [20/10/2025]. See the Terms and Conditions (https://rmets.onlinelibrary.wiley.com/doi/10.1002/qj.70044 by Institute Of Science And Technology Austria, Wiley Online Library on [20/10/2025]. See the Terms and Conditions (https://rmets.onlinelibrary.wiley.com/doi/10.1002/qj.70044 by Institute Of Science And Technology Austria, Wiley Online Library on [20/10/2025]. See the Terms and Conditions (https://rmets.onlinelibrary.wiley.com/doi/10.1002/qj.70044 by Institute Of Science And Technology Austria, Wiley Online Library on [20/10/2025]. See the Terms and Conditions (https://rmets.onlinelibrary.wiley.com/doi/10.1002/qj.70044 by Institute Of Science And Technology Austria, Wiley Online Library on [20/10/2025]. See the Terms and Conditions (https://rmets.onlinelibrary.wiley.com/doi/10.1002/qj.70044 by Institute Of Science And Technology Austria, Wiley Online Library on [20/10/2025]. See the Terms and Conditions (https://rmets.onlinelibrary.wiley.com/doi/10.1002/qj.70044 by Institute Of Science And Technology Austria, Wiley Online Library on [20/10/2025]. See the Terms and Conditions (https://rmets.onlinelibrary.wiley.com/doi/10.1002/qj.70044 by Institute Of Science And Technology Austria, Wiley Online Library on [20/10/2025]. See the Terms and Conditions (https://rmets.onlinelibrary.wiley.com/doi/10.1002/qj.70044 by Institute Of Science And Technology Austria, Wiley Online Library on [20/10/2025]. See the Terms and Conditions (https://rmets.onlinelibrary.wiley.com/doi/10.1002/qj.70044 by Institute Of Science And Technology Austria, Wiley Online Library on [20/10/2025]. See the Terms and Conditions (https://rmets.onlinelibrary.wiley.com/doi/10.1002/qj.70044 by Institute Of Science And Technology (https://rmets.onlinelibrary.wiley.com/doi/10.1002/qj.70044 by Institute Of Science And Technology (https://rmets.onlinelibrary.wiley.com/doi/10.1002/qj.70044 by Institu

ditions) on Wiley Online Library for rules of use; OA articles are governed by the applicable Creative Commons License

in the distributions of temperature and water-vapour mixing ratio (and consequently, the moist static energy). We note that, generally, plume-based models for predicting vertical velocities do not take into account large buoyancy or velocity anomalies arising within the boundary layer itself (Singh & O'Gorman, 2015). Our results thus suggest, at least within the idealised settings used here, that boundary-layer dynamics might play a role in setting in-cloud velocities in addition to the acceleration from CAPE. This result was somewhat pre-empted in AMC25. Fig. 5 of AMC25 shows that the vertical profile of w in clouds in their idealised, Direct Numerical Simulations (DNS) can be directly predicted by an initial velocity at the bottom of the cloud and the vertical integral of the in-cloud buoyancy.

3.4 | A non-dimensional scaling for moist convection

In the appendix of AMC25, the authors suggested a non-dimensionalisation of the equations on the basis of setting the rate of radiative cooling to unity. This was done by setting temperature scale \mathcal{T} and time-scale t_0 such that

$$R = \mathcal{T}t_0^{-1}. (4)$$

Through this relation, setting a time-scale automatically sets the temperature scale and vice versa. This step is justified, as in RCE it is R that sets the dynamics of the entire system. As seen in this study, the dynamics also depends strongly on the surface temperature, which determines the availability of heat and moisture in the boundary layer. Increasing the SST for the same value of R increases w_c and decreases σ and M_c . The decrease of mass flux with warming has been noted and can be seen within the references of Jeevanjee (2022). One way to interpret this decrease is that a given rate of radiative cooling must be balanced by the transport of an equal amount of heat upward by convection. This heat is either transported directly, as sensible heat, or as latent heat by the transport of moisture. A warmer plume is also more moist, allowing the transport of more latent heat for the same mass of air, thus necessitating fewer plumes to balance the same amount of cooling.

AMC25 suggested the dimensionless parameter given by

$$\mathcal{N} = \frac{c_{\rm p}RH}{q_0 U_0 L},\tag{5}$$

where c_p is the specific heat capacity of dry air, H is a vertical length-scale, q_0 is a water-vapour mixing ratio scale, U_0 is a velocity scale, and L is the latent heat of condensation of water. t_0 is then given by H/U_0 , which gives the

temperature scale from Equation (4). For the current study, we set q_0 to be q_a , or the specific humidity at the first model level closest to the surface. Given that there is no moisture flux out of the top of the domain, this value is equivalent to specifying the net condensation in the entire column. For the velocity scale U_0 , we set it to be the mid-tropospheric peak value of the vertical profile of w_c . This corresponds to a value of about $2.5 \text{ m} \cdot \text{s}^{-1}$ (see, for example, the second panel in Figure 3). The length-scale H is set to be the height at which σ goes below a small value (10^{-4}), representing the height up to which clouds reach in the simulations. We notice here that the numerator of $\mathcal N$ is similar to a net cooling-rate term for the entire height, while the denominator is similar to a rate of latent heating. It can be seen that using $t_0 = H/U_0$ and $R = \mathcal T/t_0$ gives simply

$$\mathcal{N} = \frac{c_{\rm p} \mathcal{T}}{L q_0},\tag{6}$$

where \mathcal{T} and q_0 are the appropriate temperature and water-vapour mixing ratio scales.

We study the variation of \mathcal{N} with the nondimensionalised mass flux, which we denote \hat{M}_c . We consider the height of the lower tropospheric peak in M_c as the cloud-base height, which lies above the LCL. Taking the same velocity scale U_0 and setting ρ_0 , the density scale, as the density of air at the lowest model level gives

$$\hat{M}_{\rm c} = \frac{M_{\rm c}|_{\rm cb}}{\rho_0 U_0},\tag{7}$$

where $M_{\rm c}|_{\rm cb}$ is the cloud mass flux at this cloud-base height. While definitions of the cloud base can vary in the literature, the mass flux at this level is known to play an important role in the dynamics of moist convection. The Held and Soden (2006) scaling, where precipitation is equated to the product of $M_c|_{cb}$ and the saturation specific humidity at the same height, was widely accepted until recent work (Jeevanjee, 2022; Williams & Jeevanjee, 2025) suggested that "Bett's rule" (Betts, 1998), with a prefactor of (1 - RH), where RH is the environmental relative humidity, leads to more robust predictions about the scaling of mass flux under varying climates. The water budget implies that precipitation is in turn equal to the LHF (modulo a constant related to ρ , c_p , and the latent heat of condensation of water). Given that changes in density with height across the simulations are small (see the rightmost panel of Figure 3), \hat{M}_c scales roughly as $\sigma_{ch} w_{ch}/U_0$. We have already argued that, while w in clouds close to the boundary layer is set by R and the strength of the fluxes, w in the mid-troposphere is set by a combination of the boundary-layer w and the buoyant acceleration due to condensation above the boundary layer.

FIGURE 10 Log-log plot of non-dimensional parameter \mathcal{N} versus the non-dimensionalised cloudy mass flux \hat{M}_c for the VAT, CAT simulations (red squares) and other simulations carried out with varying values of R and SST with the same setup (see Table B1). The inset shows the same plot for the DNS simulations from AMC25. [Colour figure can be viewed at wileyonlinelibrary.com]

Figure 10 shows \hat{M}_c plotted against \mathcal{N} in log-log coordinates. This is plotted for the VAT and CAT simulations (red squares) as well as an additional set of simulations (blue circles) where R and SST are varied widely using the same RCE setup. Details of the additional simulations can be found in Appendix B. Figure 10 shows that \mathcal{N} and $\hat{M}_{\rm c}$ scale well with a simple 3/4 power law. A linear fit performed for the logarithm of the values yielded a slope of 0.783. In the inset of Figure 10, we show the log-log plot of the non-dimensionalised mass flux with the same non-dimensional number ${\cal N}$ calculated for the 2D direct numerical simulations detailed in AMC25, discussed further in Appendix B. Here too, the response of the mass flux scales closely with the same power law when the imposed bulk cooling in the domain is varied by one order of magnitude. This indicates that the mass flux in moist convection, similar to the Nusselt number of Rayleigh-Bénard convection (Grossmann & Lohse, 2000; Heslot et al., 1987) and numerous other non-dimensionalised flux metrics for various other forms of convection (Klinger & Marshall, 1995; Yang et al., 2016), follows a scaling power law that is a constant in the regimes explored here.

This scaling can be rationalised and interpreted by considering that, within the setup of a typical RCE model with fixed radiative cooling such as we have here, the dynamics is only a function of R and SST. When R increases, the difference in temperature between the surface (SST) and the first atmospheric level in the model (T_a) must increase so that the surface fluxes, parametrised by bulk formulae as proportional to this difference ΔT , also increase. The latent heat flux is also proportional to the difference Δq

between the saturation mixing ratio at SST, $q^*(SST)$, and q_a . For a given SST, increasing R leads to a smaller q_a , leading to a larger increase (relative to the increase in R) in \mathcal{N} . This corresponds to the VAT simulations described in this study. On the other hand, if q_a is to be kept fixed as R is increased (decreased), then the SST must also be increased (decreased) accordingly. This corresponds to the CAT simulations described in this study.

Our empirical scaling suggests that, for fixed q_a achieved by tuning the SST, \hat{M}_c would scale roughly as $\sim R^{3/4}$, assuming small changes in U_0 and H. In the case in which R is fixed and q_a alone is varied by varying the SST, \hat{M}_c would then scale as $\sim q_a^{-3/4}$. This latter scaling is the observed decrease in cumulus mass flux for a warmer atmosphere. In fact, under a global warming scenario with higher surface temperatures and increased atmospheric CO₂ concentration, q_a is expected to increase strongly ($\sim 7\% \cdot \text{K}^{-1}$), while the increase in total R in the troposphere is expected to be slower (Held & Soden, 2006), leading to a decrease in \mathcal{N} , again assuming that changes in H and U_0 are much smaller.

We make an informed guess that the scaling would break down in two different asymptotic regimes. Firstly, if R is held to be zero but the SST is large enough, this would induce moist convection in the absence of destabilisation by radiative cooling. This is the situation, for example, in Rainy-Bénard convection (Vallis et al., 2019) and other systems of simplified moist convection (Pauluis & Schumacher, 2010). Here, \hat{M}_c is finite while \mathcal{N} is 0. In the second scenario, in a system with large R in conjunction with small SST, the system would approach dry convection and there would be no "clouds" or significant moist dynamics, thus the quantity of mass flux in clouds would be ill-defined. The behaviour of radiatively cooled, purely dry convection has been studied in Berlengiero et al. (2012) and Agasthya and Muller (2024). Finally, we note that recently an alternate non-dimensional quantity to characterise the static stability of moist convection with radiative cooling has been proposed by Dritschel et al. (2025) using CAPE calculated from the steady-state temperature profile, which depends on molecular diffusivity of air as well as the rate of radiative cooling.

4 | CONCLUSION AND DISCUSSION

In this study, we have considered the cloud-resolving model SAM in an RCE configuration with constant sea-surface temperature and with the radiative cooling idealised as a constant, bulk cooling term with rate $R \times d^{-1}$. Our setup and numerical experiments are very similar to previous work conducted in CRMs (Craig & Cohen, 2006; Robe & Emanuel, 1996) and DNS (Agasthya *et al.*, 2025).

We vary R systematically and study the response of the domain and various moist-convective parameters in the simulations, in particular the cloud mass flux, the area fraction of the domain, and the vertical velocity in clouds. To decouple the direct impact of varying R on the domain from the indirect effect of the changing temperature, we conduct an additional set of simulations where the SST is changed from simulation to achieve a nearly constant temperature profile across simulations.

We study the scaling of these convective parameters as a function of the imposed radiative cooling and find that, consistent with previous studies, the increase in cloud mass flux M_c (an increase required for energy balance) occurs by an increase in cloud area fraction σ , while the vertical velocity in clouds w_c shows only small changes. This scaling occurs in both simulations with the same surface temperature (VAT) and simulations with the same atmospheric temperature (CAT), showing that the impact of the decrease in temperature of the domain is not important in causing an increase in convective area.

Outside clouds, the dynamics is set directly by radiative cooling, with the magnitude of subsiding velocity $w_{\rm sub}$ increasing according to a theoretical balance between subsidence warming and radiative cooling as in Equation (3). However, it is pertinent to note that, while this scaling was found to hold outside clouds, $w_{\rm sub}$ defined this way is not quantitatively representative of radiative balance, as it is an order of magnitude larger than the prediction from radiative cooling. Instead, we find that the dynamics outside "convecting regions" is more akin to a pure radiative balance.

We further find that the various cloud characteristics are functions of temperature alone, independent of any changes in large-scale circulation. This constrains the buoyancy within clouds to not grow large enough to produce large vertical velocities, even when the surface fluxes are very large. The changes in vertical velocity we do observe can be explained by a combination of larger variability in the boundary layer with increasing R followed by vertical acceleration that scales broadly with CAPE above the boundary layer. The large variability in the boundary layer can be seen in the vertical velocity in clouds, where, for simulations with larger R, cloud parcels have already acquired a significant vertical velocity even before they are accelerated by CAPE. The extreme vertical velocities are also found to scale with R, similar to the average in-cloud vertical velocities.

Finally, we use a non-dimensionalisation suggested previously in AMC25 to propose a scaling for moist convection that holds true for cloud-resolving model simulations as well as direct numerical simulations. The non-dimensionalised mass flux \hat{M}_c scales as $\mathcal{N}^{3/4}$, where \mathcal{N} is the non-dimensionalised ratio between the rate of

radiative cooling R and the water-vapour mixing ratio at the surface q_a . The temperature scale is set by considering R to be of magnitude unity, while the length and velocity scales are set to be the vertical extent of moist convection in the domain and the vertical velocity in clouds, respectively. It remains to be seen to what extent the non-dimensional scaling discovered here is generally applicable to moist convection, particularly in the case where radiative cooling is not fixed externally but is represented realistically. Initial results from RCE simulations performed with fixed SST, fully interactive radiation, and changing CO_2 by the authors indicate that the 3/4 power-law relationship also holds in this case, though the parameter space explored was fairly narrow.

A key aspect that needs further investigation is the scope and relevance of the current study. It remains to be understood whether the slow change in vertical velocity and strong response of cloud area to varying large-scale forcing studied and characterised here should be interpreted as a Tropics-wide change in RCE or can also be seen over smaller time- and length-scales. The applicability of RCE simulation results to the Earth's atmosphere has been vigorously debated (Romps, 2021; Seeley & Romps, 2015; Singh & O'Gorman, 2013) and the results here are not immune from this debate. This gap could be bridged by assessing global climate model outputs, particularly storm-resolving models (Stevens et al., 2019), which resolve deep convection without parametrisations. Non-equilibrium studies of limited-domain models of moist convection are also a candidate to shed further light on this topic. An interesting question to ask is: under what model conditions could few clouds with large w_c be generated as a response to increasing R?

In this study, we have taken a step in moving towards unifying studies on highly idealised prototypes of convection with more realistic models. This family of models ranges from classical Rayleigh–Bénard convection to realistic regional and global climate models, with various degrees of idealisations, simplifications, and parametrisations in between. Fundamental studies of moist convection and general convection hold several insights into the behaviour of the Earth's atmosphere, whether for dry convection, shallow moist convection, or deep moist convection.

ACKNOWLEDGEMENTS

The authors gratefully acknowledge discussions with Professor Robert Plant (University of Reading, UK), Professor Steve Sherwood (University of New South Wales, Australia), Professor Steve Tobias, Professor Douglas Parker, and Gregory Dritschel (University of Leeds, UK). Discussions with colleagues at the Institute of Science and Technology Austria played a large role in shaping this

study. The authors are particularly grateful for inputs and discussions from Dr. Jiawei Bao, Dr. Alejandro Casallas, and Alzbeta Pechacova.

This project has received funding from the European Union's Horizon 2020 research and innovation programme under the Marie Sklodowska–Curie grant agreement No. 101034413. C. Muller gratefully acknowledges funding from the European Research Council (ERC) under the European Union's Horizon 2020 research and innovation program (Project CLUSTER, Grant Agreement No. 805041). This research was supported by the Scientific Service Units (SSU) of IST Austria through resources provided by Scientific Computing (SciComp). Open Access funding provided by Institute of Science and Technology Austria/KEMÖ.

CONFLICTS OF INTEREST STATEMENT

The authors report no conflict of interest.

DATA AVAILABILITY STATEMENT

The data that support the findings of this study are available from the corresponding author, L. Agasthya, upon reasonable request.

ENDNOTE

¹We thank Professor Robert Plant for suggesting this elegant terminology.

ORCID

Lokahith Agasthya https://orcid.org/0000-0001-8689

Caroline Muller https://orcid.org/0000-0001-5836-5350

REFERENCES

- Agasthya, L., Muller, C. & Cheve, M. (2025) Moist convective scaling: insights from an idealised model. *Quarterly Journal of the Royal Meteorological Society*, 151, e4902. Available from: https://doi.org/10.1002/qj.4902
- Agasthya, L. & Muller, C.J. (2024) Dynamics and scaling of internally cooled convection. *Communications in Nonlinear Science and Numerical Simulation*, 134, 108011.
- Arakawa, A. & Schubert, W.H. (1974) Interaction of a cumulus cloud ensemble with the large-scale environment, Part I. *Journal of the Atmospheric Sciences*, 31, 674–701.
- Arakawa, A. & Wu, C.-M. (2013) A unified representation of deep moist convection in numerical modeling of the atmosphere. Part I. *Journal of the Atmospheric Sciences*, 70, 1977–1992.
- Berlengiero, M., Emanuel, K., Von Hardenberg, J., Provenzale, A. & Spiegel, E. (2012) Internally cooled convection: a fillip for Philip. *Communications in Nonlinear Science and Numerical Simulation*, 17, 1998–2007.
- Betts, A.K. (1998) Climate-convection feedbacks: some further issues. *Climatic Change*, 39, 35.
- Bony, S., Stevens, B., Coppin, D., Becker, T., Reed, K.A., Voigt, A. et al. (2016) Thermodynamic control of anvil cloud amount. *Proceedings of the National Academy of Sciences*, 113, 8927–8932.

- Bretherton, C.S., Blossey, P.N. & Khairoutdinov, M. (2005) An energy-balance analysis of deep convective self-aggregation above uniform SST. *Journal of the atmospheric sciences*, 62, 4273–4292.
- Cohen, B.G. & Craig, G.C. (2006) Fluctuations in an equilibrium convective ensemble. Part II: numerical experiments. *Journal of the atmospheric sciences*, 63, 2005–2015.
- Craig, G.C. & Cohen, B.G. (2006) Fluctuations in an equilibrium convective ensemble. Part I: theoretical formulation. *Journal of the atmospheric sciences*, 63, 1996–2004.
- Dritschel, G.N., Tobias, S.M., Parker, D.J. & Tomassini, L. (2025) Radiatively-cooled moist convection under an idealised climate change scenario: linear analysis. arXiv preprint arXiv:2504.06019.
- Emanuel, K.A. (1994) *Atmospheric convection*. USA: Oxford University Press.
- Grossmann, S. & Lohse, D. (2000) Scaling in thermal convection: a unifying theory. *Journal of Fluid Mechanics*, 407, 27–56.
- Held, I.M. & Soden, B.J. (2006) Robust responses of the hydrological cycle to global warming. *Journal of Climate*, 19, 5686–5699.
- Heslot, F., Castaing, B. & Libchaber, A. (1987) Transitions to turbulence in helium gas. *Physical Review A*, 36, 5870–5873.
- Holloway, C.E., Wing, A.A., Bony, S., Muller, C., Masunaga, H., L'Ecuyer, T.S. et al. (2017) Observing convective aggregation. Surveys in Geophysics, 38, 1199–1236.
- Houze, R.A., Jr. (2004) Mesoscale convective systems. Reviews of Geophysics, 42, RG4003. Available from: https://doi.org/10.1029 /2004RG000150
- Jakob, C., Singh, M. & Jungandreas, L. (2019) Radiative convective equilibrium and organized convection: an observational perspective. *Journal of Geophysical Research: Atmospheres*, 124, 5418–5430.
- Jeevanjee, N. (2022) Three rules for the decrease of tropical convection with global warming. *Journal of Advances in Modeling Earth Systems*, 14, e2022MS003285.
- Jeevanjee, N. & Fueglistaler, S. (2020) Simple spectral models for atmospheric radiative cooling. *Journal of the Atmospheric Sciences*, 77, 479–497.
- Jeevanjee, N. & Zhou, L. (2022) On the resolution-dependence of anvil cloud fraction and precipitation efficiency in radiative-convective equilibrium. *Journal of Advances in Modeling Earth Systems*, 14, e2021MS002759.
- Johns, R.H. & Doswell, C.A., III. (1992) Severe local storms forecasting. *Weather and Forecasting*, 7, 588–612.
- Khairoutdinov, M.F. & Randall, D.A. (2003) Cloud resolving modeling of the arm summer 1997 IOP: model formulation, results, uncertainties, and sensitivities. *Journal of the Atmospheric Sciences*, 60, 607–625.
- Kiladis, G.N., Wheeler, M.C., Haertel, P.T., Straub, K.H. & Roundy, P.E. (2009) Convectively coupled equatorial waves. *Reviews of Geophysics*, 47, RG2003. Available from: https://doi.org/10.1029/2008RG000266
- Klinger, B.A. & Marshall, J. (1995) Regimes and scaling laws for rotating deep convection in the ocean. *Dynamics of Atmospheres and Oceans*, 21, 227–256.
- Manabe, S. & Strickler, R.F. (1964) Thermal equilibrium of the atmosphere with a convective adjustment. *Journal of the Atmospheric Sciences*, 21, 361–385.
- Muller, C.J. & Held, I.M. (2012) Detailed investigation of the self-aggregation of convection in cloud-resolving simulations. *Journal of the Atmospheric Sciences*, 69, 2551–2565.
- Muller, C.J. & O'Gorman, P. (2011) An energetic perspective on the regional response of precipitation to climate change. *Nature Climate Change*, 1, 266–271.

- Muller, C.J., O'Gorman, P.A. & Back, L.E. (2011) Intensification of precipitation extremes with warming in a cloud-resolving model. *Journal of Climate*, 24, 2784–2800.
- Parodi, A. & Emanuel, K. (2009) A theory for buoyancy and velocity scales in deep moist convection. *Journal of the Atmospheric Sciences*, 66, 3449–3463.
- Pauluis, O. & Garner, S. (2006) Sensitivity of radiative–convective equilibrium simulations to horizontal resolution. *Journal of the Atmospheric Sciences*, 63, 1910–1923.
- Pauluis, O. & Schumacher, J. (2010) Idealized moist Rayleigh-Bénard convection with piecewise linear equation of state. *Communications in Mathematical Sciences*, 8, 295–319.
- Rayleigh, L. (1916) LIX on convection currents in a horizontal layer of fluid, when the higher temperature is on the under side. *The London, Edinburgh, and Dublin Philosophical Magazine and Journal of Science*, 32, 529–546.
- Robe, F.R. & Emanuel, K.A. (1996) Moist convective scaling: some inferences from three-dimensional cloud ensemble simulations. *Journal of Atmospheric Sciences*, 53, 3265–3275.
- Romps, D.M. (2014) An analytical model for tropical relative humidity. *Journal of Climate*, 27, 7432–7449.
- Romps, D.M. (2021) Ascending columns, WTG, and convective aggregation. *Journal of the Atmospheric Sciences*, 78, 497–508.
- Seeley, J.T., Jeevanjee, N., Langhans, W. & Romps, D.M. (2019) Formation of tropical anvil clouds by slow evaporation. *Geophysical Research Letters*, 46, 492–501.
- Seeley, J.T. & Romps, D.M. (2015) Why does tropical convective available potential energy (cape) increase with warming? *Geophysical Research Letters*, 42, 10–429.
- Shutts, G. & Gray, M. (1999) Numerical simulations of convective equilibrium under prescribed forcing. *Quarterly Journal of the Royal Meteorological Society*, 125, 2767–2787.
- Singh, M.S. & Neogi, S. (2022) On the interaction between moist convection and large-scale ascent in the tropics. *Journal of Climate*, 35, 4417–4435.
- Singh, M.S. & O'Gorman, P.A. (2012) Upward shift of the atmospheric general circulation under global warming: theory and simulations. *Journal of Climate*, 25, 8259–8276.
- Singh, M.S. & O'Gorman, P.A. (2013) Influence of entrainment on the thermal stratification in simulations of radiative-convective equilibrium. *Geophysical Research Letters*, 40, 4398–4403.
- Singh, M.S. & O'Gorman, P.A. (2015) Increases in moist-convective updraught velocities with warming in radiative-convective equilibrium. *Quarterly Journal of the Royal Meteorological Society*, 141, 2828–2838. Available from: https://doi.org/10.1002/qj.2567
- Stauffer, C.L. & Wing, A.A. (2022) Properties, changes, and controls of deep-convecting clouds in radiative-convective equilibrium. *Journal of Advances in Modeling Earth Systems*, 14, e2021MS002917. Available from: https://doi.org/10.1029/2021MS002917
- Stevens, B. (2005) Atmospheric moist convection. Annual Review of Earth and Planetary Sciences, 33, 605–643. Available from: https://doi.org/10.1146/annurev.earth.33.092203.122658
- Stevens, B., Satoh, M., Auger, L., Biercamp, J., Bretherton, C.S., Chen, X. et al. (2019) Dyamond: the dynamics of the atmospheric general circulation modeled on non-hydrostatic domains. *Progress in Earth and Planetary Science*, 6, 1–17.
- Tompkins, A.M. & Craig, G.C. (1998) Radiative–convective equilibrium in a three-dimensional cloud-ensemble model. *Quarterly Journal of the Royal Meteorological Society*, 124, 2073–2097.

- Vallis, G.K., Parker, D.J. & Tobias, S.M. (2019) A simple system for moist convection: the Rainy–Bénard model. *Journal of Fluid Mechanics*, 862, 162–199.
- Williams, A.I. & Jeevanjee, N. (2025) A robust constraint on the response of convective mass fluxes to warming. *Journal of Advances in Modeling Earth Systems*, 17, e2024MS004695.
- Wing, A.A., Emanuel, K., Holloway, C.E. & Muller, C. (2017) Convective self-aggregation in numerical simulations: a review. In: *Shallow Clouds, Water Vapor, Circulation, and Climate Sensitivity*, Space Science Series of ISSI, 65, 1–25.
- Wing, A.A. & Emanuel, K.A. (2014) Physical mechanisms controlling self-aggregation of convection in idealized numerical modeling simulations. *Journal of Advances in Modeling Earth Systems*, 6, 59–74. Available from: https://doi.org/10.1002/2013MS000269
- Yang, Y., Verzicco, R. & Lohse, D. (2016) Scaling laws and flow structures of double diffusive convection in the finger regime. *Journal of Fluid Mechanics*, 802, 667–689.
- Yano, J.-I. & Plant, R. (2012) Finite departure from convective quasi-equilibrium: periodic cycle and discharge–recharge mechanism. Quarterly Journal of the Royal Meteorological Society, 138, 626–637.
- Zhang, C. (2005) Madden-Julian oscillation. *Reviews of Geo*physics, 43, RG2003. Available from: https://doi.org/10.1029 /2004RG000158

How to cite this article: Agasthya, L. & Muller, C. (2025) Moist convection and radiative cooling: Dynamical response and scaling. *Quarterly Journal of the Royal Meteorological Society*, e70044. Available from: https://doi.org/10.1002/qj.70044

APPENDIX A. ISOTHERMAL COORDINATES

The scaling of moist convective and other quantities is plotted at fixed temperature levels rather than fixed height at various points in the main text. Previous studies (Robe & Emanuel, 1996) compared w_c , σ , and M_c at the same height. However, this captures different convective dynamics in different simulations. In Figure A1, we plot the profiles from Figures 2 and 3 in isothermal coordinates, that is, using the average temperature profile as the vertical coordinate. We note several features of interest. Firstly, despite very different conditions in the sub-cloud layer in the VAT simulations, all the profiles of relative humidity are nearly invariant with temperature across simulations in the mid-troposphere. The basic physics behind this RH-T invariance has been studied before (Romps, 2014).

The cloud base can be discerned by looking at the lower tropospheric maximum of the cloud area fraction (which is the same as the maximum in M_c). For the VAT simulations, this cloud base occurs at very different temperatures. However, the mid-tropospheric peaks in w_c are much

1477870x, 0, Downloaded from https:

library.wiley.com/doi/10.1002/qj.70044 by Institute Of Science And Technology Austria,

Wiley Online Library on [20/10/2025]. See the Terms

on Wiley Online Library for rules of use; OA articles are governed by the applicable Creative Commons Licenso

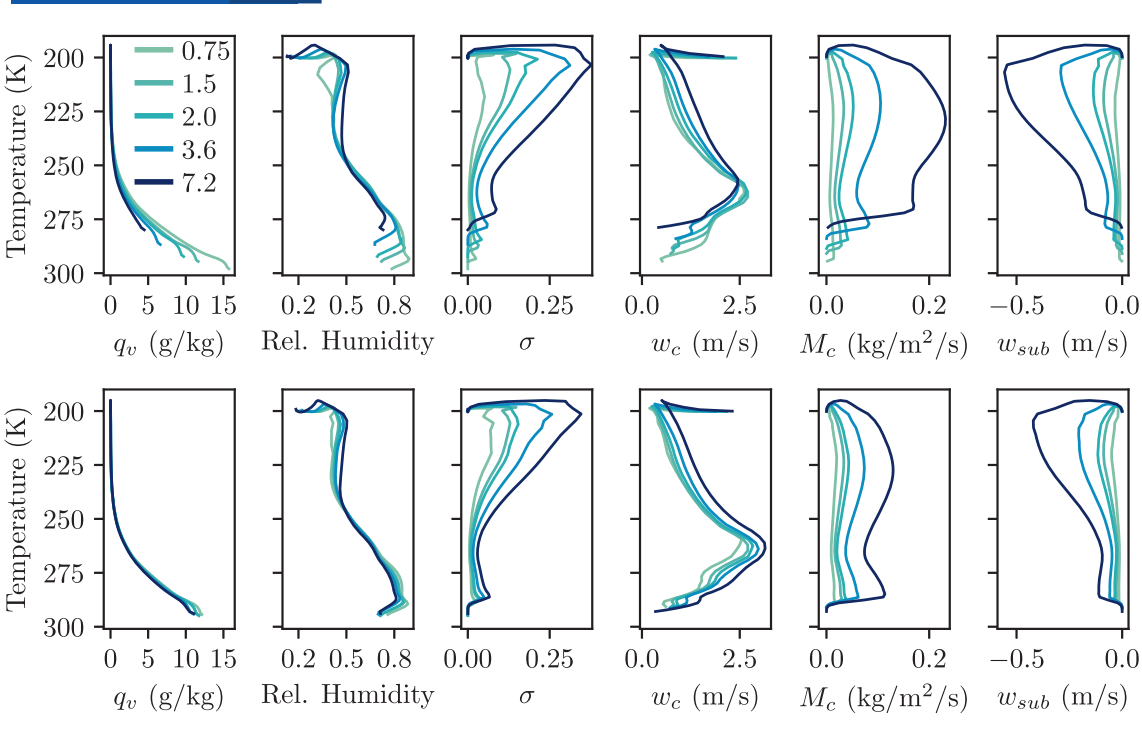


FIGURE A1 From left to right: time- and horizontally averaged profiles of water-vapour mixing ratio q_v , relative humidity, cloud area fraction σ , vertical velocity in clouds w_c , cloud mass flux M_c , and vertical velocity outside clouds w_{sub} for VAT simulations (top panels) and CAT simulations (bottom panels). The profiles are plotted against the averaged temperature profile, that is, in isothermal coordinates. [Colour figure can be viewed at wileyonlinelibrary.com]

closer together, shifting slightly upward for larger R. The upper peak in σ , which corresponds closely to the minimum of $w_{\rm sub}$, is the cloud anvil and this too occurs at a roughly fixed temperature, independent of the lower tropospheric temperature. This is expected, however, given that we enforce a fixed stratospheric temperature of 200 K. We choose a temperature level close to 250 K for our analysis, as this is close to the peak of w_c and is in a regime where the cloud area is increasing with height, influenced purely by in-cloud processes.

In the CAT simulations, due to the temperature profiles being nearly identical, all the curves have the same shape in the vertical when plotted in isothermal coordinates as when they are plotted as a function of height.

APPENDIX B. NON-DIMENSIONAL SCALING

In addition to the VAT and CAT simulations, we performed RCE simulations with fixed radiative cooling R and constant SST across a wider range of parameters to understand the scaling of the non-dimensional parameters $\mathcal N$ and $\hat M_c$ introduced in Section 3.4. The values of R and SST chosen are listed in Table B1.

TABLE B1 List of parameters *R* and SST for which additional simulations with the same setup were performed to obtain the points in Figure 10.

$R(\mathbf{K}\cdot\mathbf{d}^{-1})$	SST (K)
0.5	(295, 305, 310)
2	(295, 305, 310)
6	(295, 305, 310)
10	(290,295, 305, 310)

For the DNS simulations of moist convection, the velocity scale was chosen as the usual diffusive velocity as given in AMC25, while the length-scale was simply the height of the domain. For q_0 , the water-vapour mixing ratio at z=1 was chosen, while for \hat{M}_c the mass flux was assessed at z=5 in the simulation units of their study. For q_a , z=1 corresponded to a height above the diffusive boundary in all the simulations. The peak of M_c was close to z=5, since the DNS simulations were performed assuming constant density (Boussinesq approximation) rather than decreasing with height.